International Scientific Journal
Environmental Science
http://environment.scientific-journal.com

Experimental Investigation of Impingement Heat Transfer on a Smooth and Helical Shaped Ribs Plate

Mehmet Eren
Department of Mechanical Engineering
Hitit University
Corum, Turkey
mehmeteren@hitit.edu.tr

Sinan Caliskan
Department of Mechanical Engineering
Hitit University
Corum, Turkey
sbycaliskan@gmail.com

***Abstract*— Impingement heat transfer is considered as a promising heat transfer enhancement technique. Impinging jets have received considerable attention during the last decade. The reason is mainly due to their inherent characteristics of high rates of heat transfer besides having simple geometry. Among all convection heat transfer enhancement methods, it provides significantly high local heat transfer coefficient. Due to their widespread applications ranging from electronics equipment and turbine blade cooling to drying of textiles and glass tempering, impinging jets have been studied extensively in the literature. The heat transfer measurement over a surface with helical shaped ribs by a circular impinging jet was investigated using thermal infrared camera. Jet in the array should exhibit the same initial velocity profile. A plenum section is constructed that met this demand. The impingement section is open on all four sides providing free outflow of the spent air. The rib pitch (p) to rib height (e) ratio is 4.6. Helices were cut from aluminum material has a diameter of 100 mm. During the experiments, the different Reynolds number and different jet-to-plate distance spacing was studied. The heat transfer results of the helical shaped ribs are compared with those of a smooth plate. The presence of the helical shaped ribs on the target plate produce higher heat transfer coefficients than the smooth plate.**

Keywords*— *Helical shaped ribs; Confined impinging jets; Heat transfer; Infrared camera.

I. INTRODUCTION

Heat transfer enhancement is getting higher importance since last few years. Impingement heat transfer is considered as an attractive heat transfer enhancement technique. Impinging jets are widely used where the high rate of heat transfer are required. Impinging jets are used for heating, cooling and drying purposes. Applications include cooling of electronic components, gas turbine blade cooling, drying of textiles, and heating or cooling of metal plates.

First studies dealt with uniformly heated square or rectangular channels with two opposite rib-roughened walls; continuous, regularly spaced, transverse ribs have been the most common ribbed geometry for years. [1] There are many parameters which play a considerable role in the heat transfer mechanism of jet impingement. Some of these parameters are rib height, rib pitch, channel aspect ratio, hydraulic diameter, Reynolds number, etc.

The flow field of smooth surfaces and surfaces with V-shaped ribs were investigated with a Laser-Doppler Anemometry system by Caliskan and Baskaya. [2]. Reynolds stress is higher for the V-SR surfaces as compared to smooth surfaces for low jet-to-plate distances. They found that the Nusselt numbers are higher for the V-SR surfaces as compared to smooth surfaces.

The effect of turbulence on the heat transfer between two-dimensional jet and flat plate studied by Gardon and Akfirat et al. [3]. They also studied the heat transfer distribution due to impingement of two-dimensional jets. [4]. Hansen and Webb were studied the effect of the modified surface on the average heat transfer between impinging circular jet and the smooth plate.[5]. They obtained enhancements in the heat transfer relative to a smooth surface ranging from 1.5 to 4.5 times.

Caliskan [6] investigated heat transfer and flow characteristics under impingement of a multiple circular jet array with perforated rib surfaces (PRS) and solid rib surfaces (SRS) with an infrared thermal imaging technique and a Laser-Doppler Anemometry system, respectively.

In this study, helical shaped ribs have been designed. In order to determine the heat transfer of circular impinging jet for helical shaped ribs surface and smooth plates, an experimental set-up was established.

II. EXPERIMENTAL SETUP

The schematic lay-out of the experimental set-up is shown in Fig. 1. The equipment for the experiments consist of blower, frequency controller, plenum section, impinging jet plate, an infrared thermal imaging system, and data software system. The required flow rate of air has been supplied by a centrifugal blower. In order to obtain the desired flow rate for the range of Reynolds numbers of interest, a frequency controller has been connected to the blower. The plenum is a 1250 mm long rectangular duct with an inner rectangular cross section of 100x150 mm. In order to measure the plenum air temperature is used a K-type thermocouple. Circular sharp-edged hole are used to generate the impinging jets. Its

diameter d is equal to 5 mm. A uniform flow was achieved at the jet exit. The infrared thermograph system, which includes a ThermaCAM SC500 camera from FLIR systems and a PC with AGEMA Researcher software, can measure temperatures from -20 C^o to 1200 C^o with an accuracy of ±2%.

The target plate was made of stainless steel foil. It is firmly clamped and stretched between two copper bus bars. Views of the helical shaped ribs plate is shown in Fig.2. helical shaped ribs are actively transferring heat since they are made of high conductivity aluminum material. The helical shaped ribs are attached to the stainless steel foil plates by a thin layer of super-glue, with negligible contact resistance. The thermal contact resistance due to the super-glue will introduce a minor conservative bias to the reported results [7]. Thermal images are obtained from IR camera positioned on the bottom of the heater assembly vertical to the impinging jet. One-dimensional energy balance across the heated plate shows negligible temperature difference across its cross section. Hence, the local temperature measured on the bottom side is considered to be the same as that on the impingement plate.

In order to confirm the equal temperatures at the bottom and upper side of the 0.02mm thickness stainless steel foil, each surface was equipped with 2, 30-gauge copper-constantan thermocouples, attached along the center line of the target plate. All thermocouples were fixed with a thermal adhesive. All values of Reynolds numbers were considered for each surface at a fixed heat flux of 2700W/m^2. Thermal images are obtained from IR camera positioned on the bottom of the heater assembly vertical to the impinging jet.

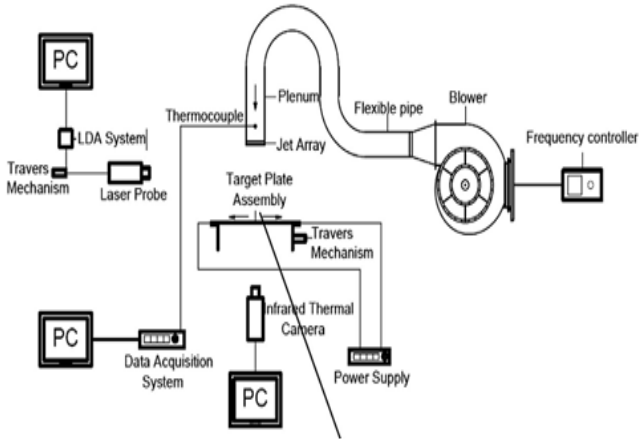

(a) Experimental set-up schematic view

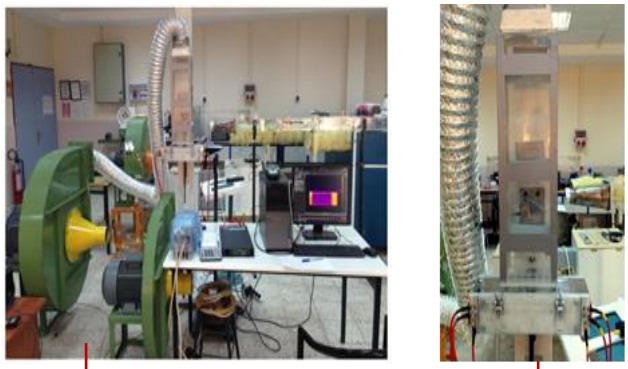

(b) Experimental set-up assembly and test section

Fig. 1. Experimental set-up: **(a)** schematic view; **(b)** assembly and test section

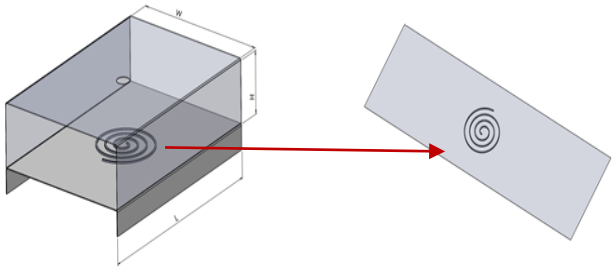

(a) A channel with helical shaped rib

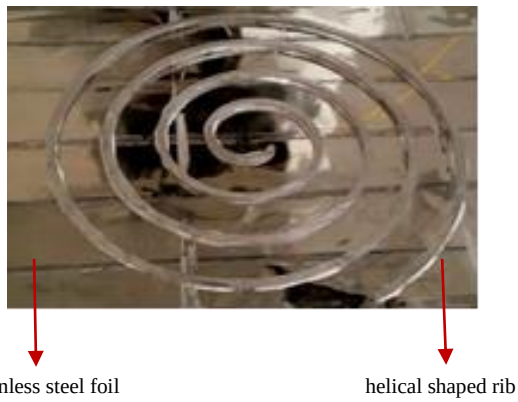

(b) Top view of the helical shaped rib

Fig. 2. Schematic view of present ribs: **(a)** a channel with helical shaped ribs; **(b)** top view of the helical shaped rib

The bottom side of the stainless steel foil is covered with a layer of black backing paint. The emissivity of each side of the plate was measured with an AE anemometer and was found to be 0.82 and 0.13 for the painted and unpainted surfaces, respectively. All thermocouples were fixed with a thermal adhesive. The plate surface temperature was measured with the infrared camera and compared with the thermocouple readings.

Local heat transfer coefficients (h_i) can be calculated considering the following energy balance:

$$q_e = q_j + q_r + q_f + q_c \quad (1)$$

The electrically generated heat flux q_e was transferred to the environment by forced convection q_j, radiation q_r, free convection q_f and conduction in the metal sheet q_c.

In Eq. 1, the electrical heat flux (q_e) can be calculated with the following equation

$$q_e = \frac{VI}{A} \quad (2)$$

In Eq. 2, V is the voltage on the sheet, I is the current through the sheet, and A is the area of the heated surface.

Radiation, free convection and conduction were considered as heat losses. The radiation heat flux from both sides of the sheet is given by

$$q_r = (\varepsilon_t + \varepsilon_b)\sigma\left(T^4 - T_s^4\right) \quad (3)$$

where ε_t and ε_b are the emissivities of the painted and unpainted surfaces, respectively. σ is the Stefan-Boltzmann constant.

The free convection heat flux was calculated using

$$q_f = h_f\left(T - T_s\right) \quad (4)$$

where the free convection coefficient h_f was defined as 1.1 W/m^2K for an air velocity of 0.1 m/s [8].

The conduction loss is given by:

$$q_c = k\frac{\Delta T}{t} \quad (5)$$

where k is thermal conductivity of the sheet, ΔT is the temperature difference across the sheet, and t is the thickness of the sheet. Because of the thinness of the sheet, lateral conduction is negligible as reported by Lytle and Webb [9]. The conduction, free convection and radiation losses were found to be less than 7.4 %.

The heat flux by forced convection of the jet flow was defined by

$$q_j = h_i(T - T_j) \quad (6)$$

where h_i is the local heat transfer coefficient, T is the sheet temperature, and T_j is the jet exit temperature.

The local Nusselt number is calculated from:

$$Nu = \frac{h_i\, d}{k_{air}} \quad (7)$$

where d is the jet diameter and k_{air} is the thermal conductivity of air.

The jet Reynolds number is defined as,

$$\mathrm{Re} = \frac{W_{jet}\, d}{\nu} \quad (8)$$

where W_{jet} is the average jet velocity at the jet exit and d is the inner jet diameter, ν is the kinematic viscosity of air. Thermo physical properties were evaluated at the average of jet inlet and plate temperatures, except for the viscosity in the Reynolds number which was calculated at the jet inlet temperature.

The uncertainty in the experimental data was determined according to the procedure proposed by Kline and McClintock [10].

III. RESULTS AND DISCUSSION

The effect of Reynolds number on the stagnation point Nusselt number is presented for various H/d values in Fig. 3. In all the cases considered in the experimental study, the stagnation point Nusselt number decreases monotonically as the H/d increases. Hence it is concluded that the heat transfer rate is higher at low H/d ratio. A similar trend was observed by Sparrow et al. [11] and Tawfek [12]. For the jet-to-plate spacing of H/d=4.0, the impinging jet shows complex heat transfer characteristics in stagnation region due to reflection, sudden change of flow direction and interaction between the impinging jet and the heated flat plate. As shown in Fig.3 the differences between maximum and minimum stagnation point Nusselt numbers is nearly constant for H/d=2 and H/d=4.

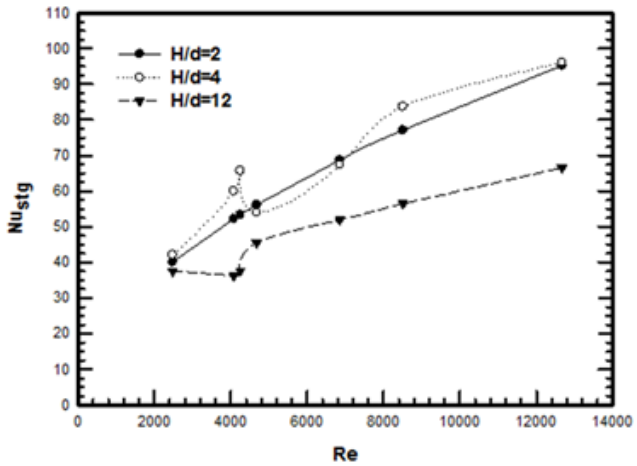

Fig. 3. Reynolds number vs stagnation point Nusselt number at H/d = 2, 4, and 12.

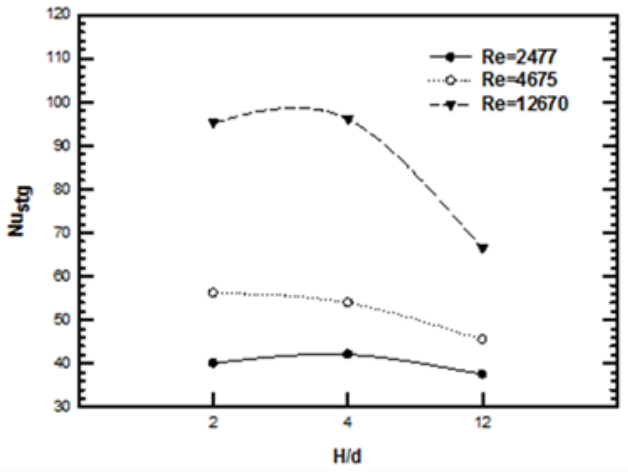

Fig. 4. The variation of stagnation Nusselt number with H/d

Fig. 4 represents the stagnation point Nusselt number values for different Reynolds number. The lowest stagnation point Nusselt number value is obtained for H/d=12. For Fig. 3 and 4, the Nusselt numbers at the stagnation points decrease with increase of H/d.

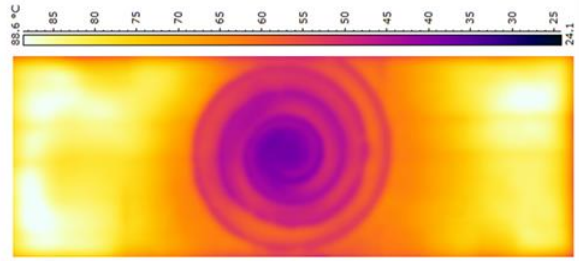

(a) Re=4675, H/d=2, helical shaped ribs plate

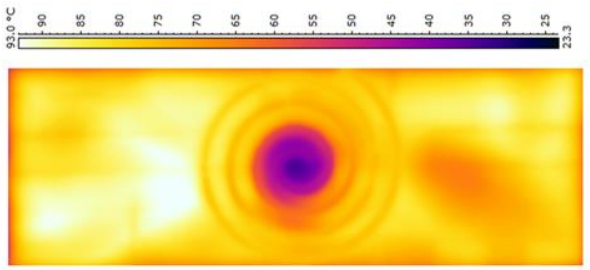

(b) Re=4675, H/d=4, helical shaped ribs plate

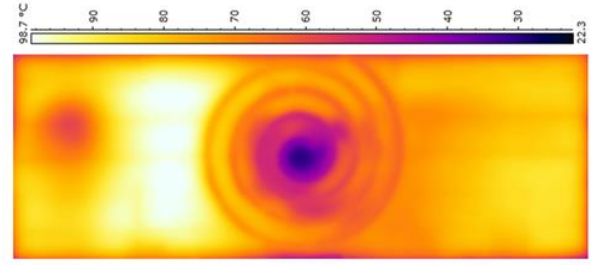

(c) Re=4675, H/d=12, helical shaped ribs plate

Fig. 5. Temperature (°C) field obtained for different jet-to-plate distance and Re=4675.

The temperature contour obtained for Re=4675 and different H/d=2, 4 and 12 are presented in Fig. 5, respectively. As shown in Fig. 5, the stagnation point Nusselt numbers are higher. Also heat transfer at wall jet regions is higher. High Nusselt number values are obtained on stagnation points and around stagnation points the Nusselt numbers are degrading gradually. At the wall jet regions a larger difference was observed compared to the stagnation points.

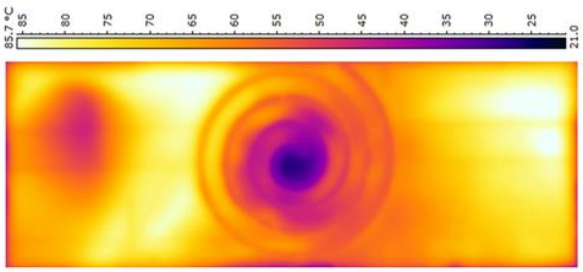

(a) Helical shaped rib surface, Re=12670, H/d=2

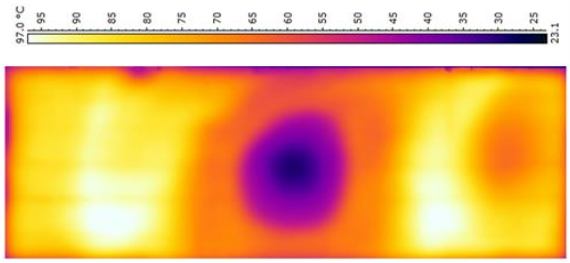

(b) Smooth surface, Re=12670, H/d=2

Fig. 6. Contour maps showing distribution of surface temperature due to jet impingement on smooth surface with and without helical shaped rib at Re = 12670 and H/d=2.0

Contour maps due to jet impingement on a smooth surface with helical ribs for the same H/d and Reynolds number are shown in Fig. 6. The comparison of the two figures for a given H/d and Reynolds number indicates that heat transfer coefficients around the stagnation point are higher with the helical rib surface.

Temperature contours for Re=2477, 4675, 12670 and H/d=2 are presented in Fig. 7. As can be seen, from all figures, the Re=12670 and H/d=2 provides higher heat transfer coefficients than the other Reynolds number. The potential core length of for the lower Reynolds is shorter than that of higher Reynolds number. This attributes to the strong mixing and large spreading rate of higher Re number compared to lower Re number. As shown in Fig. 7, the jet axis shift increases with increasing jet-to-plate distance.

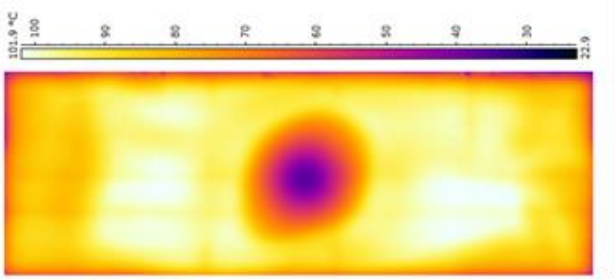

(a) Re=2477, H/d=2, smooth plate

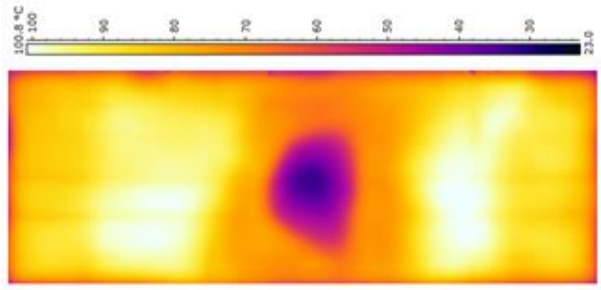

(b) Re=4675, H/d=2, smooth plate

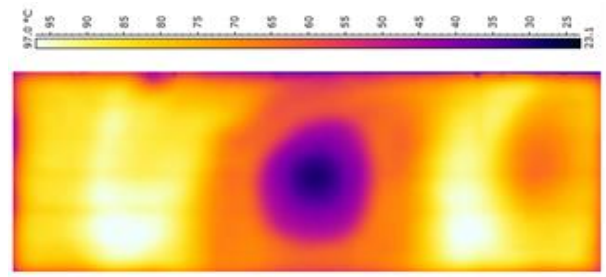

(c) Re=12670, H/d=2, smooth plate

Fig. 7. Surface temperature distributions at different Reynolds number and constant H/d

IV. CONCLUSIONS

The heat transfer characteristics in a single impingement jet on smooth and helical shaped ribs plate are investigated in the present study. Nusselt number distributions have been measured on the target plate using a thermal infrared camera. The main conclusions that can be drawn from the present study are as follows:

- The heat transfer performance was found to be highest for an H/d of 2 and Reynolds number of 12670.
- Helical shaped ribs plate provides higher heat transfer coefficients than smooth surface.

ACKNOWLEDGMENTS

The present work is financially supported by Hitit University (Grant No.MUH19003.14.001).

SYMBOLS

A	Area (m^2)
d	Jet diameter (m)
e	Height of rib (m)
H/d	Distance between the plate and the jet exit (-)
h_f	Free convection heat transfer coefficient ($W/m^2 K$)
h_i	Local convection heat transfer coefficient ($W/m^2 K$)
L	length of test channel (m)
I	Current (Ampere)
k	Thermal conductivity of the sheet (W/m K)
k_{air}	Thermal conductivity of air (W/m K)
Nu	Nusselt number (-)
Nu_{stg}	Stagnation Nusselt number (-)
q_c	Conduction heat flux (W/m^2)
q_j	Convection heat flux (W/m^2)
q_e	Electrical power (W/m^2)
q_f	Free convection heat flux (W/m^2)
q_r	Radiation heat flux (W/m^2)
p	spacing between ribs (m)
Re	Jet Reynolds number at the jet exit (-)
ΔT	Temperature difference across the sheet (ºC)
T_j	Jet exit temperature (ºC)
T	Heated wall temperature (ºC)
T_S	Ambient temperature (ºC)
W_{jet}	Mean velocity at the jet exit (m/s)
Greek symbols	
ε	Emissivity
σ	Stefan-Boltzmann-constant (W/ m^2K^4)
Subscripts	
air	Air
jet	jet inlet
stg	Stagnation

REFERENCES

[1] J.C. Han, P.R. Chandra, and S.E. Lau, Local Heat/Mass Transfer Distributions around Sharp 180 Deg Turn in Two-Pass Smooth and Rib-Roughened Channels, ASME 1. Heat Transfer 110, 91-98 (1988)

[2] S. Caliskan, S. Baskaya, Velocity field and turbulence effects on heat transfer characteristics from surfaces with V-shaped ribs, Int. J. Heat Mass Transfer 55 (2012) 6260–6277.

[3] R. Gardon, C. Akfirat, The role of turbulence in determining the heat transfer characteristics of impinging jets, Int. J. Heat Mass Transfer 8 (1965) 1261–1272.

[4] R. Gardon, C. Akfirat, Heat transfer characteristics of impinging two dimensional air jets, J. Heat Transfer 88 (1966) 101–108.

[5] L.G. Hansen, B.W. Webb, Air jet impingement heat transfer from modified surfaces, Int. J. Heat Mass Transfer 36 (1993) 989–997.

[6] S. Caliskan, Flow and heat transfer characteristics of transverse perforated ribs under impingement jets, Int. J. Heat Mass Transfer 66 (2013) 244-260.

[7] A.P. Rallabandi, D.H. Rhee, Z. Gao, J.C. Han, Heat transfer enhancement in rectangular channels with axial ribs or porous foam under through flow and impinging jet conditions, Int. J. Heat Mass Transfer 53 (2010) 4663–4671 .

[8] L.P.B.M. Janssen, M.M.C.G. Warmoeskerken, Transport Phenomena-Data Companion, DUM, Delft 2 (1991).

[9] D. Lytle, B.W. Webb, Air jet impingement heat transfer at low nozzle plate spacings, Int. J. Heat Mass Transfer 37 (1994) 1687–1697.

[10] S.J. Kline, F.A. McClintock, Describing uncertainties in single-sample experiments, Mech. Eng. 73 (1953) 3–8.

[11] E.W. Sparrow, C.A.C. Altemani, A. Chaboki, Jet-impingement heat transfer for a circular jet impinging in crossflow on a cylinder, ASME Journal of Heat Transfer 106 (1984) 570–577.

[12] A.A. Tawfek, Heat transfer due to round jet impinging normal to a circular cylinder, Heat and Mass Transfer 35 (1999) 327–333.